STUDY ON FAILURE CHARACTERISTICS OF GEAR TRANSMISSION SYSTEM WITH CRACK FAULT

Xin WANG[1]

In order to investigate the characteristics of crack fault in a gear transmission system, dimensionless dynamical equations of the gear transmission system which contains a two-stage fixed-axis gear with crack fault and a one-stage planetary gear were established and solved by a numerical method. The bifurcation diagrams, phase diagrams, Poincaré sections and frequency spectrums in two conditions (normal and crack) is contrasted, so as to obtain the bifurcation characteristics of the system, and the failure frequency characteristics. The numerical simulation results are used to identify the fault of test rig.

Keywords: gear transmission system, nonlinear dynamical, crack fault, bifurcation

1. Introduction

Crack is a common fault of gear transmission system. The study of this kind of fault is one of the problems in the current gear system dynamics. At present, the research on the cracked gears has not been theoretical, and the failure model and analysis results are not accurate enough and need further study.

In recent years, some scholars have studied the vibration mode, natural frequency and meshing stiffness of crack fault by finite element simulation [1-2]. However, the mechanism of crack failure needs to be studied though the nonlinear perspective. Ma Rui [3-4] established a torsional dynamic model of monopole gear with crack fault, and analyzed the dynamic characteristics caused by gear crack fault. Zhang Qingfeng [5] simulated the crack fault in tooth root by time-varying meshing stiffness, and established a nonlinear dynamic fault model with crack fault in tooth root. Wang Yangang [6] analyzed the nonlinear dynamic behavior of single-pair gear system under different fault parameters. In this paper, the research on the root crack is based on the monopole gear and lack of the research on the failure mechanism in the whole system. In the gear transmission system, the gears will be coupled with each other to make the crack failure characteristics changed. The research results of the monopole gear cannot be applied to the multi-stage gear transmission system. Therefore, it becomes very meaningful to establish the dynamic model of the multi-stage gear transmission system with crack fault, study the dynamic mechanism of the crack fault, and find out the characteristics of crack fault in the multi-stage gear transmission system. It

[1] Dr., School of Mechanical Engineering, Baoji University of Arts and Sciences, Baoji, 721016, China, e-mail: pan_00@163.com

also provides a solid theoretical basis for multi-stage gear transmission system fault diagnosis.

2. Torsional dynamic model of gear transmission system

The system studied in this paper is a test rig of gear transmission system which contains a two-stage fixed-axis gear and a one-stage planetary. Where spur gears 1, 2 compose the 1st stage fixed-axis gear for the input, spur gears 3, 4 compose the 2nd stage fixed-axis gear, the planet carrier is for the output. The torsional dynamic model is established by using the lumped mass method as shown in Fig. 1. The model does not consider the transverse vibration displacement of gears. Gear meshing parameter is simulated with a spring and a damper.

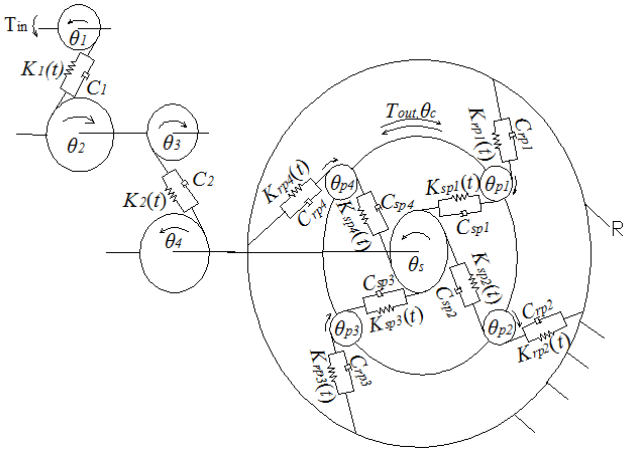

Fig.1. Torsional dynamic model of gear transmission system

here, θ_s, θ_c, θ_{pn}, θ_1, θ_2, θ_3, θ_4 represent the angular displacement of sun gear, planet carrier, planetary gear n (n=1, 2, 3, 4), spur gears 1, 2, 3, 4, respectively. Throughout this paper, the subscripts s, c, pn, r, 1, 2, 3, 4 denote sun gear, planet carrier, planetary, ring gear and squr gears 1, 2, 3, 4. Quantities r_s, r_c, r_{pn}, r_1, r_2, r_3, r_4 are the base circle radius of gears. Quantities $K_{spn}(t)$, $K_{rpn}(t)$, $K_1(t)$, $K_2(t)$ denote the meshing stiffness of sun gear with planetary gear n, ring gear with planetary gear n, 1st stage fixed gear and 2nd stage fixed gear. Quantities C_{spn}, C_{rpn}, C_1, C_2 denote the damping of sun gear with planetary gear n, ring gear with planetary gear n, 1st stage fixed gear and 2nd stage fixed gear. T_{in} is the input and T_{out} is the output.

2.1 Motion differential equations of the system

Based on the Lagrangian equation, the motion differential equation of the system shown in Fig. 1 is established on the basis of the clearance, the time-

varying meshing stiffness and the comprehensive meshing error.

$$\begin{cases} J_1\ddot{\theta}_1 + r_1F_1 = T_{in} \\ J_{23}\ddot{\theta}_2 - r_2F_1 + r_3F_2 = 0 \\ J_{4s}\ddot{\theta}_{4s} + \sum_{n=1}^{4} r_sF_{spn} - r_4F_2 = 0 \\ J_{pn}\ddot{\theta}_{pn} - r_{pn}F_{spn} + r_{pn}F_{rpn} = 0 \\ J_c\ddot{\theta}_c - \sum_{n=1}^{4} r_cF_{spn} - \sum_{n=1}^{4} r_cF_{rpn} = -T_{out} \end{cases} \tag{1}$$

Here, $J_{23} = J_2 + J_3$, $J_{4s} = J_4 + J_s$, where J_1, J_2, J_3, J_4, J_s, J_{pn}, J_c are the mass moments of inertia of each gear on the shaft;

F_1, F_2, F_{spn}, F_{rpn} are the meshing force of each stage on the meshing line, $F_i = C_i\dot{x}_i + K_i(t)f(x_i)$, ($i$=1, 2, *spn*, *rpn*);

x_i is the relative displacement of each stage meshing line, (i=1, 2, *spn*, *rpn*),

$x_1 = r_1\theta_1 - r_2\theta_2 - e_1(t)$, ; $x_2 = r_3\theta_3 - r_4\theta_4 - e_2(t)$,

$x_{spn} = r_s\theta_s - r_{pn}\theta_{pn} - r_c\theta_c - e_{spn}(t)$, $x_{rpn} = r_{pn}\theta_{pn} - r_c\theta_c - e_{rpn}(t)$;

$f(x_i)$ is the clearance nonlinear function, (i=1, 2, *spn*, *rpn*), written as

$$f(\bar{x}_i) = \begin{cases} \bar{x}_i - b_i, & \bar{x}_i > b_i \\ 0, & |\bar{x}_i| \le b_i \\ \bar{x}_{rpi} + b_i, & \bar{x}_i < -b_i \end{cases} \tag{2}$$

where, b_i is half of the clearance, (i=1, 2, *spn*, *rpn*).

The time-varying meshing stiffness of the gear pair $K_i(t)$ will be specified in 2.2.

The damping coefficients form as

$$\begin{aligned} C_1 &= 2\xi_1\sqrt{K_{m1}/(1/m_1 + 1/m_2)} \\ C_2 &= 2\xi_2\sqrt{K_{m2}/(1/m_3 + 1/m_4)} \\ C_{spn} &= 2\xi_{spn}\sqrt{K_{mspn}/(1/m_s + 1/m_{pn})} \\ C_{rpn} &= 2\xi_{rpn}\sqrt{K_{mrpn}/(1/m_r + 1/m_{pn})} \end{aligned} \tag{3}$$

where, ξ_1, ξ_2, ξ_{spn}, ξ_{rpn} are damping ratio and m_1, m_2, m_3, m_4, m_s, m_{pn}, m_r are the mass of each gear.

The comprehensive meshing error of gear pair using the 1st harmonic form of meshing function, that is

$$e_i(t) = e_{ai}\sin(w_{mi}t + \varphi_i) \tag{4}$$

Here, e_{ai} is the comprehensive meshing error amplitude of each gear, (i=1, 2, *spn*, *rpn*), and φ_i is the comprehensive meshing error initial phase of each gear, (i=1, 2, *spn*, *rpn*). w_{mi} is the meshing frequency of each gear, (i=1, 2, *spn*, *rpn*).

Define time nominal scale w_h, order $\tau = w_ht$, where $w_h = \sqrt{K_{m1} \times m_{e1}}$.

Dimensionless displacement is $\bar{x}_i = x_i / b_1$, i=1, 2, *spn*, *rpn*. Dimensionless excitation frequency is Ω_i, $\Omega_i = w_{mi} / w_h$, i=1, 2, *spn*, *rpn*. Dimensionless comprehensive meshing error amplitude is $\bar{e}_{ai} = e_{ai} / b_1$, i=1, 2, *spn*, *rpn*. Dimensionless nonlinear function is:

$$f(\bar{x}_i) = \begin{cases} \bar{x}_i - b_i / b_1, & \bar{x}_i > b_i / b_1 \\ 0, & |\bar{x}_i| \le b_i / b_1 \\ \bar{x}_{rpi} + b_i / b_1, & \bar{x}_i < -b_i / b_1 \end{cases} \tag{5}$$

The equations are normalized, and the system dimensionless motion differential equations can be obtained as:

$$\begin{cases} \ddot{\bar{x}}_1 + \dfrac{C_1}{m_{e1} w_h} \dot{\bar{x}}_1 + \dfrac{K_1(\tau)}{m_{e1} w_h^2} f(\bar{x}_1) - \dfrac{C_2}{m_{e2} w_h} \dot{\bar{x}}_2 - \dfrac{K_2(\tau)}{m_{e2} w_h^2} f(\bar{x}_2) = \dfrac{T_{in} r_1}{J_1 w_h^2 b_1} + \dfrac{e_{a1}}{b_1} \Omega_1^2 \sin(\Omega_1 \tau + \varphi_1) \\ \ddot{\bar{x}}_2 - \dfrac{C_1}{m_{e1} w_h} \dot{\bar{x}}_1 - \dfrac{K_1(\tau)}{m_{e2} w_h^2} f(\bar{x}_1) + \dfrac{C_2}{m_{e3} w_h} \dot{\bar{x}}_2 + \dfrac{K_2(\tau)}{m_{e3} w_h^2} f(\bar{x}_2) - \sum_{n=1}^{4} \dfrac{C_{spn}}{m_{4s} w_h} \dot{\bar{x}}_{spn} - \sum_{n=1}^{4} \dfrac{K_{spn}(\tau)}{m_{4s} w_h^2} f(\bar{x}_{spn}) = \dfrac{e_{a2}}{b_1} \Omega_2^2 \sin(\Omega_2 \tau + \varphi_2) \\ \ddot{\bar{x}}_{spn} + \dfrac{1}{m_{4s} w_h} \sum_{n=1}^{4} C_{spn} \dot{\bar{x}}_{spn} + \dfrac{1}{m_c w_h} \sum_{n=1}^{4} C_{spn} \dot{\bar{x}}_{spn} + \dfrac{1}{m_{pn} w_h} C_{spn} \dot{\bar{x}}_{spn} + \dfrac{1}{m_{4s} w_h^2} \sum_{n=1}^{4} K_{spn}(\tau) f(\bar{x}_{spn}) + \dfrac{1}{m_c w_h^2} \sum_{n=1}^{4} K_{spn}(\tau) f(\bar{x}_{spn}) \\ + \dfrac{1}{m_{pn} w_h^2} K_{spn}(\tau) f(\bar{x}_{spn}) - \dfrac{1}{m_{pn} w_h} C_{rpn} \dot{\bar{x}}_{rpn} + \dfrac{1}{m_c w_h} \sum_{n=1}^{4} C_{rpn} \dot{\bar{x}}_{rpn} - \dfrac{1}{m_{pn} w_h^2} K_{rpn}(\tau) f(\bar{x}_{rpn}) + \dfrac{1}{m_c w_h^2} \sum_{n=1}^{4} K_{rpn}(\tau) f(\bar{x}_{rpn}) \\ - \dfrac{r_4 C_2}{m_{4s} r_s w_h} \dot{\bar{x}}_2 - \dfrac{r_4 K_2(\tau)}{m_{4s} r_s w_h^2} f(\bar{x}_2) = \dfrac{r_c T_{out}}{J_{ce} w_h^2 b_1} + \dfrac{e_{aspn}}{b_1} \Omega_{spn}^2 \sin(\Omega_{spn} \tau + \varphi_{spn}) \\ \ddot{\bar{x}}_{rpn} - \dfrac{1}{m_{pn} w_h} C_{spn} \dot{\bar{x}}_{spn} + \dfrac{1}{m_c w_h} \sum_{n=1}^{4} C_{spn} \dot{\bar{x}}_{spn} - \dfrac{1}{m_{pn} w_h^2} K_{spn}(\tau)(\bar{x}_{spn}) + \dfrac{1}{m_c w_h^2} \sum_{n=1}^{4} K_{spn}(\tau) f(\bar{x}_{spn}) + \dfrac{1}{m_{pn} w_h} C_{rpn} \dot{\bar{x}}_{rpn} \\ - \dfrac{1}{m_c w_h} \sum_{n=1}^{4} C_{rpn} \dot{\bar{x}}_{rpn} + \dfrac{1}{m_{pn} w_h^2} K_{rpn}(\tau) f(\bar{x}_{rpn}) - \dfrac{1}{m_c w_h^2} \sum_{n=1}^{4} K_{rpn}(\tau) f(\bar{x}_{rpn}) = \dfrac{r_c T_{out}}{J_{ce} w_h^2 b_1} + \dfrac{e_{arpn}}{b_1} \Omega_{rpn}^2 \sin(\Omega_{rpn} \tau + \varphi_{rpn}) \end{cases} \tag{6}$$

where m_{e1}, m_{e2}, m_{e3}, m_{4s} are the equivalent mass of gear, J_{ce} is the equivalent mass moment of inertia of gear,

$$m_{e1} = \frac{J_1 J_{23}}{J_{23} r_1^2 + J_1 r_2^2} , \; m_{e2} = \frac{J_{23}}{r_2 r_3} , \; m_{e3} = \frac{J_4 J_{23}}{J_{23} r_4^2 + J_4 r_3^2} , \; m_{4s} = \frac{J_{4s}}{r_s^2} ; \; J_{ce} = J_c + N m_{pn} r_c^2 .$$

2.2 Mesh stiffness

Yang and Lin [7] proposed the potential energy method to calculate the mesh stiffness of a pair of external–external spur gears by considering Hertzian contact stiffness k_h, bending stiffness k_b and axial compressive stiffness k_a. Later, Tian et al. [8] introduced an additional term called the shear stiffness k_s in the potential energy method. Their expressions are more concise and clear in form and easy to be programed, and therefore is used in this paper to calculate gear tooth stiffness K_t. This method is also the most widely used method. Chen [9], Yu [10], Anand Parey [11] and Liang [12] applied this method to calculate the gear

crack. The cracked tooth model is shown in Fig. 2.

2.2.1 Overall mesh stiffness

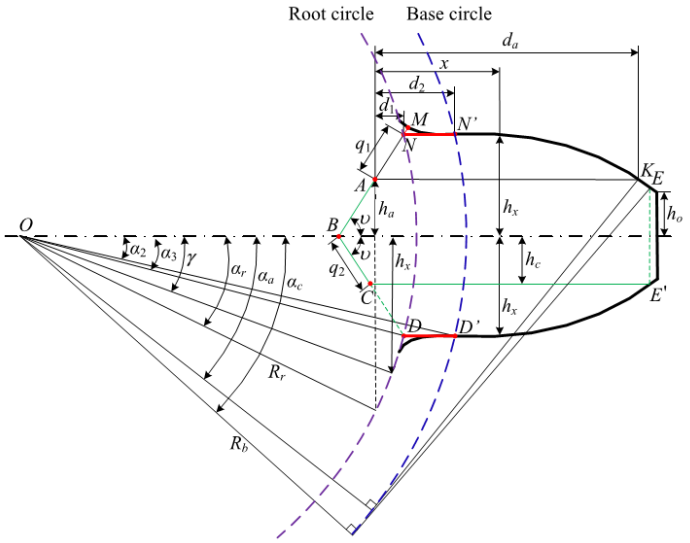

Fig.2. Cracked tooth model

Gear tooth profile follows an involute curve up to the base circle. The tooth profile between the base circle and the root circle is not an involute curve and hard to be describe analytically [13]. Therefore, straight lines NN' and DD' are used to simplify the curve. For the single-tooth-pair meshing duration, the total effective mesh stiffness can be calculated as [14]:

$$K_t = \frac{1}{\frac{1}{k_h}+\frac{1}{k_{b1}}+\frac{1}{k_{s1}}+\frac{1}{k_{a1}}+\frac{1}{k_{b2}}+\frac{1}{k_{s2}}+\frac{1}{k_{a2}}} \tag{7}$$

where subscripts 1 and 2 represent the driving gear and the driven gear, respectively.

For the double-tooth-pair meshing duration, there are two pairs of gears meshing at the same time. Total effective mesh stiffness can be obtained as [14]:

$$K_t = K_{t1} + K_{t2} = \sum_{j=1}^{2} \frac{1}{\frac{1}{k_{h,j}}+\frac{1}{k_{b1,j}}+\frac{1}{k_{s1,j}}+\frac{1}{k_{a1,j}}+\frac{1}{k_{b2,j}}+\frac{1}{k_{s2,j}}+\frac{1}{k_{a2,j}}} \tag{8}$$

where j=1 for the 1st pair and j=2 for the 2nd pair of meshing teeth.

2.2.2 Crack modeling

Lewichi [15] found that several factors such as rim and web thicknesses, initial crack location and backup ratio (rim thickness divided by tooth height) decided the gear crack propagation. Belsak and Flasker [16] investigated the propagation path of the crack both experimentally and computationally. The results indicated that the crack propagation paths were smooth, continuous, and in

most cases, rather straight with only a slight curvature, similar to the findings in Ref. [15]. It is pointed out by both Kramberger et al. [17] and Belsak and Flasker [16] that the crack mostly initiated at the point of the maximum principle stress in the tensile side of a gear tooth (critical area in Fig. 2).

The crack is modeled as a straight line from the gear tooth danger area, as shown in Fig. 2. The crack propagates along the straight line until reaching the tooth central line at point B. Then, it changes the propagation direction towards point D where the tooth breaks. According to the state of the crack in the test rig, only the state when the crack does not reach the centerline is studied, where q_1 is the crack length and the angle between the crack line and the tooth center line is defined as υ.

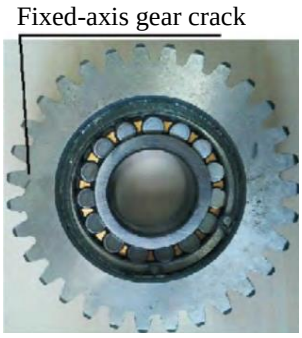

Fig.3. The fixed-axis gear with crack

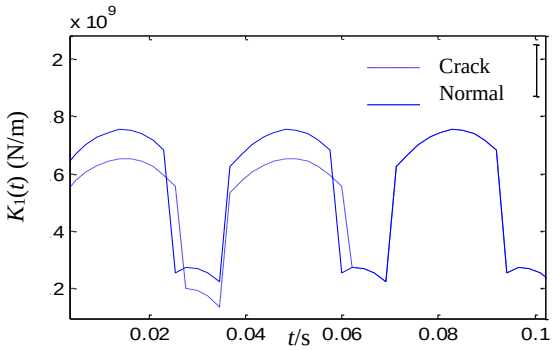

Fig. 4. The meshing stiffness of the fixed axis gear with crack

Table 1

Gear parameters

Gear	Number of tooth	R_{ri} [mm]	R_{bi} [mm]	Mass m_i [g]	J_i [g·m^2]	Face width [mm]
1	29	19.2	20.4	125	0.05	30
2	100	68.9	70.5	1224.5	6	30
3	36	23.9	25.3	224	0.14	30
4	90	61.5	63.4	1111	4	20
s	28	12.3	13	41	0.007	20
pn	36	16	17	34.6	0.01	20
c			30	848.7	0.76	20
r	100	45.6	47			20

The Hertzian stiffness and axial compressive stiffness will not be affected by the crack propagation [14]. Only the bending stiffness and the shear stiffness will be affected due to the change in the tooth length and the tooth height caused by the crack.

In this study, we assume that the 1st stage fixed-axis small gear (spur gear 1) has a crack fault. The crack gear in test rig is shown in Fig. 3 (crack length q_1 = 1mm, crack angle υ= 70°). The time varying meshing stiffness is calculated when the speed is 1Hz, as shown in Fig. 4 below. The gear parameters of gear

transmission system as shown in Table 1.

3 Nonlinear Dynamic Behavior Analysis of Fixed-axis Crack Fault

The bifurcation diagrams with the excitation frequency changed are calculated respectively when the system is in normal state and fixed-axis crack state. The structure parameters of the system are shown in Table 1 and 2, pressure angle α_0=20°, T_{in}=6.5N·m, T_{out}=8.5N·m. The values in Table 2 are the same on the meshing line of gear, so the subscript i is omitted.

Table 2

Parameters of calculation

Parameters of calculation	Value
Gear clearance b(μm)	5
comprehensive meshing error amplitude e_a(μm)	2
Meshing pair damping ratio ξ	0.07
Gear contact ratio	1.68

As the fault occurs at the 1st stage fixed-axis pinion gear, the fault feature at the meshing point of the 1st stage fixed-axis is more obvious, so the bifurcation diagram is studied on this point. The nonlinear differential Eqs. (6) are numerically solved using the variable step Runge-Kutta method to obtain the bifurcation diagram of the relative displacement of the 1st stage fixed-axis gear, in normal state and fixed-axis crack fault state with the dimensionless excitation frequency Ω_1 changed, as shown in Fig. 5.

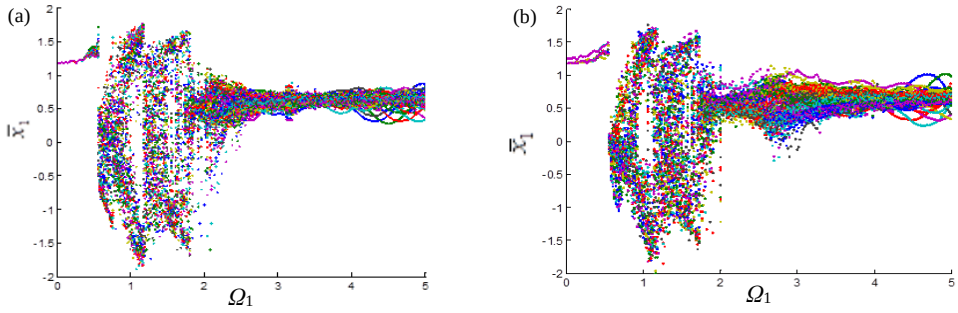

Fig.5. Displacement bifurcation diagram of the first fixed gear (a) normal state, (b) fixed-axis crack fault state

The 1st stage fixed-axis gear is periodic motion when the excitation frequency is very small (Fig. 5a). When the excitation frequency Ω_1 increases to 0.57, the system changes periodic motion to chaos by crisis jump. “Crisis jump” refers to the phenomenon that the number or size of chaotic attractors changes suddenly when the system control parameters slowly change. Previous studies have shown that with the change of system parameters, attractive chaos and non-attractive chaos can be transformed into each other through crisis jump. The phenomenon has been repeated in the numerical simulation of rigid cubic nonlinear systems and systems with clearance [18]. The chaotic interval amplitude

decrease when the excitation frequency Ω_1=1.9. It changes from chaos to quasi-periodic motion when the excitation frequency Ω_1=3.

Compared with Figs. 5a and b, the failure of the 1st stage fixed-axis crack makes the single-periodic motion before the crisis at the meshing point of the 1st stage fixed-axis gear becomes double periodic motion. The extra periodic is the fault period. The newly added fault period can also be seen in the interval of the excitation frequency [3,4], but can not be revealed in the chaotic interval.

As the actual motor speed is usually 0 ~ 50Hz, so select the situation when the fault periodic is obvious and the excitation frequency is small (Ω_1=0.5, corresponding to the motor speed 15Hz) for analysis. The nonlinear characteristics of the system in the normal state and fault state are obtained in Fig. 6 and 7. The dimensionless characteristic frequencies of gear transmission system at all levels are shown in Table 3.

Table 3

Dimensionless characteristic frequencies of gear transmission system (Hz)

Characteristic frequency	Dimensionless frequency
Meshing frequency of 1st stage fixed-axis gear f_1	1
Meshing frequency of 2nd stage fixed-axis gear f_2	0.3599
Meshing frequency of planetary f_3	0.0877
Fault frequency of 1st stage fixed-axis gear f_d	0.0345

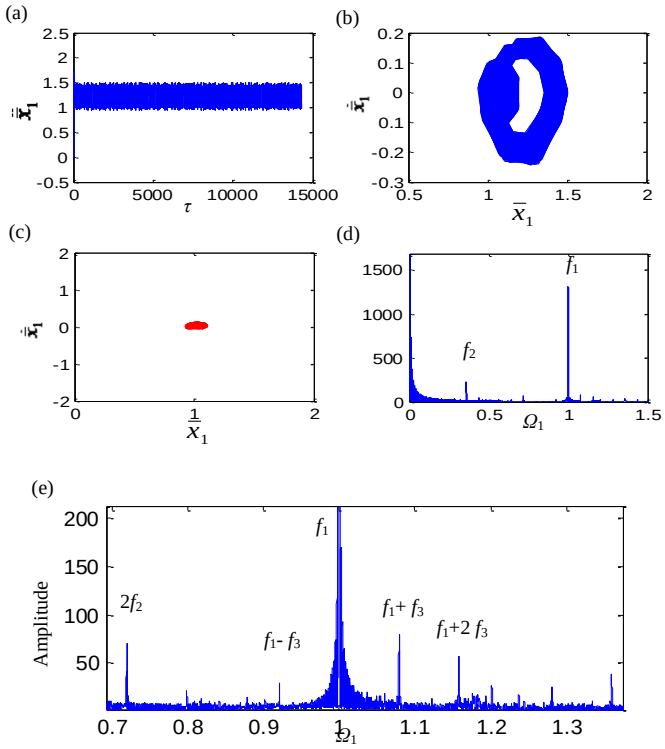

Fig.6. Nonlinear characteristics of the system under normal state at Ω_1=0.5 (a) Displacement, (b) Phase Diagram, (c) Poincaré section, (d) Frequency spectrum, and (e) Frequency thinning spectrum.

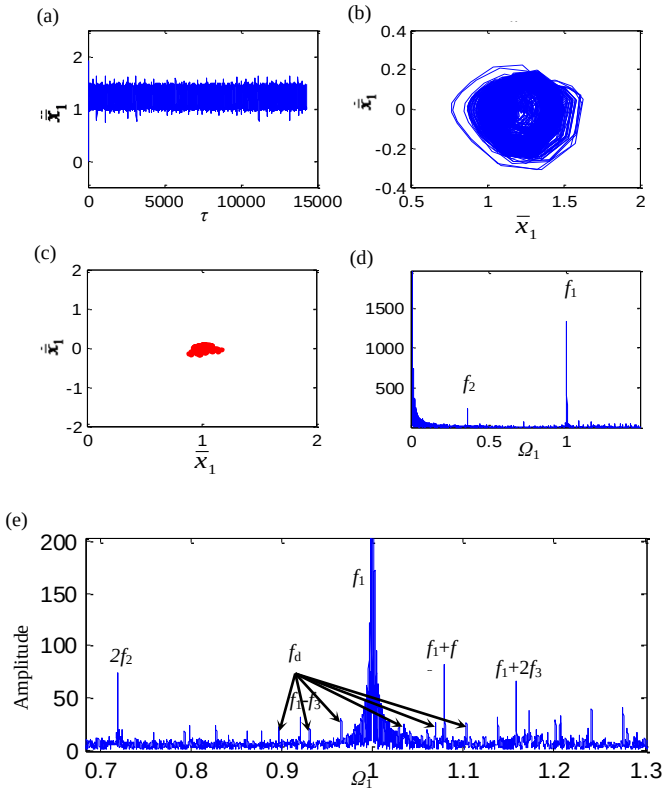

Fig.7. Nonlinear characteristics of the system under fixed-axis gear crack state at Ω_1=0.5 (a) Displacement, (b) Phase Diagram, (c) Poincaré section, (d) Frequency spectrum, and (e) Frequency thinning spectrum.

Compared with Figs. 6 and 7, the system is in periodic motion when the normal state Ω_1=0.5. The crack failure increases the oscillation in original steady amplitude in the time domain (Fig. 6a). The single cycle ring is filled in the phase diagram (Fig. 6b) and the point group is increased in the Poincaré section (Fig. 6c). In the spectrum thinning diagram of Figs. 6e and 7e, the increase in the crack of the fixed-axis causes the edge frequencies around the 1st stage fixed-axis meshing frequency f_1 to increase. The edge frequencies are all the fault frequency of 1st stage fixed-axis f_d caused by the fixed-axis crack fault.

4 Analysis of Experimental Failure

The test rig of gear transmission system which contains a two-stage fixed-axis gear and a one-stage planetary is shown in Fig. 8. The parameters are shown in Table 1 and 3. Testing and analyzing the signal of the test rig in normal state and fixed-axis crack fault state, in which, the crack failure occurs on the 1st stage pinion (spur gear 1 in Fig. 1) with the crack length q_1=1mm and the crack angle υ=70°. Sampling frequency is 3000Hz, the number of sampling points is 2048,

and the axial measurement points of the fixed-axis gear box drive side are selected for testing.

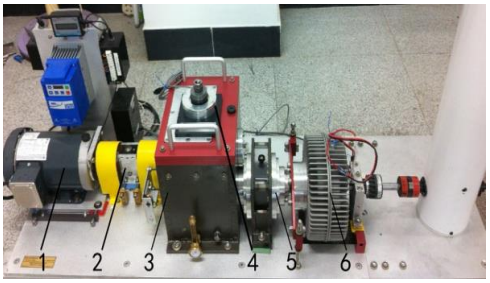

1-Motor, 2-Torque sensor and encoder, 3-Two stage fixed-axis gearbox, 4-Radial load of bearing, 5-One stage planetary gearbox, 6-Brake

Fig.8. The test rig of gear transmission system

In order to do a comparative analysis with the numerical simulation, test and analyse the signals on the motor speed of 15Hz. In order to facilitate the comparison, the spectrums are normalized to get the dimensionless spectrum in normal state and fixed-axis crack failure state (Fig. 9).

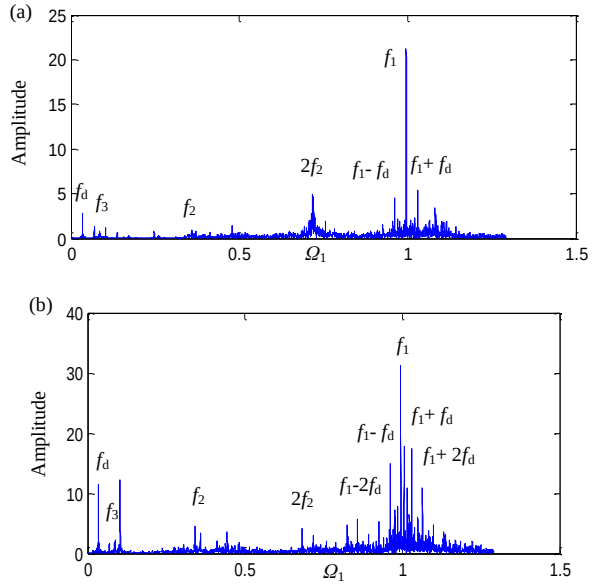

Fig.9. Dimensionless Fourier spectrum of the system (a) normal state (b) fixed-axis crack fault state

The test signal is axial and the numerical simulation signal is in the direction of the meshing line. There is a difference between the two. Contrasting Figs. 9a and 6d, the motor frequency f_d and its multiplier appear in the test signal, as well as the frequency $f_1 \pm f_d$ around the 1st stage fixed-axis meshing frequency f_1. These frequency characteristics are the vibration characteristics caused by the connection of the motor to the fixed-axis gearbox, which are not considered in the numerical simulation. In normal state, the main peak frequency of the system is

the 1st stage fixed-axis gear meshing frequency f_1, the 2nd stage fixed-axis gear meshing frequency f_2, the planetary meshing frequency f_3, as well as double frequency $2f_2$. Since the measuring point is on the 1st stage fixed-axis gear, the meshing frequency of the 1st stage fixed-axis is the highest. In general, the main peaks of the numerical simulation results are consistent with the test signal, indicating that the modeling results are reasonable and the numerical simulation results can qualitatively reflect the nonlinear characteristics of the system to a certain extent.

According to the numerical simulation results, it can be seen that the failure of the fixed-axis causes a large number of 1st stage fixed-axis fault frequency f_d around the 1st stage fixed-axis meshing frequency. Contrasting Fig. 9a and b, the amplitude of the system increases under the condition of fixed-axis crack, and the side frequencies increase around the 1st stage fixed-axis meshing frequency f_1, where appears a large number of fault frequency $f_1 \pm nf_d$ and the amplitude of side frequency increases. By comparing the fault side frequency characteristics of the simulation results with the measured signal, the fixed-axis crack fault in the measured signal is diagnosed. The diagnosis result is consistent with the failure of the test rig.

5 Conclusion

(1) The nonlinear dynamic model of the gear transmission system which contains a two-stage fixed-axis gear with crack fault and a one-stage planetary gear are established and solved by the Runge-Kutta method to get the nonlinear dynamic response of 1st stage fixed-axis gear in normal state and fixed-axis crack fault.

(2) The fixed-axis crack fault makes the single-cycle motion become a 2-cycle motion, and the periodical motion intervals before and after the chaos are obvious. But the fault period cannot be revealed in the chaotic interval.

(3) In the spectrum, the fixed-axis crack fault is manifested as the 1st stage fixed-axis fault frequency f_d around the 1st stage fixed-axis meshing frequency f_1. The failure characteristics of the test rig are identified by the numerical simulation. The diagnostic result is consistent with the test rig fault.

Acknowledgment

This research is supported by the key project of Baoji University of Arts and Sciences (209010861).

REFERENCES

[1] *R. P. Shao, W. L. Guo, M. J. Liu*, "Analysis and simulation of dynamic in characteristic for cracked gear", Mechanical Science and Technology for Aerospace Engineering, **vol. 22**, no. 5, 2003, pp. 788-791.

[2] *Y. C. Zhang, R. P. Shao, H. Y. Liu*, "The influences of crack fault to dynamic characteristics in gear transmission system", Machinery Design&Manufacture, **vol. 10**, no. 10, 2006, pp. 12-14.
[3] *R. Ma, Y. S. Chen*, "Nonlinear dynamic research on gear system with cracked failure", Chinese Journal of Mechanical Engineering, **vol. 47**, no. 21, 2011, pp. 84-90.
[4] *R. Ma, Y. S. Chen*, "Dynamic analysis of multi-freedom gear system with cracked failure", Journal of Daqing Petroleum Institute, **vol. 36**, no. 3, 2012, pp. 110-114.
[5] *Q. F. Zhang, L. W. Tang, H. Q. Zheng*, "Nonlinear dynamic fault model of gear transmission system with gear tooth crack", Journal of Vibration Engineering, **vol. 24**, no. 3, 2011, pp. 294-298.
[6] *Y. G. Wang, H. Q. Zheng, T. Q. Yang*, "Nonlinear dynamic behavior of gear system with fault parameters", Journal of Vibration, Measurement&Diagnosis, **vol. 31**, no. 5, 2011, pp. 570-574.
[7] *D. C. H. Yang, J. Y. Lin*, "Hertzian damping, tooth friction and bending elasticity in gear impact dynamics", Journal of Mechanical Design, **vol. 109**, no. 2, 1987 ,pp. 189-196.
[8] *X. H. Tian*, "Dynamic simulation for system response of gearbox including localized gear faults", Master's Thesis, University of Alberta, Edmonton, Alberta, Canada, 2004.
[9] *Z. G. Chen, Z. F. Zhu, Y. M. Shao*, "Fault feature analysis of planetary gear system with tooth root crack and flexible ring gear rim", Engineering Failure Analysis, 49, 2015, pp. 92-103.
[10] *W. N. Yu, Y. M. Shao, C. K. Mechefske*, "The effects of spur gear tooth spatial crack propagation on gear mesh stiffness", Engineering Failure Analysis, 54, 2015, pp. 103-119.
[11] *Y. Pandya, A. Parey*, "Experimental investigation of spur gear tooth mesh stiffness in the presence of crack using photoelasticity technique", Engineering Failure Analysis, 34, 2013, pp. 488-500.
[12] *X. H. Liang, M. J. Zuo, M. Pandey*, "Analytically evaluating the influence of crack on the mesh stiffness of a planetary gear set", Mechanism and Machine Theory, **vol. 76**, 2014, pp. 20-38.
[13] *A. Kapelevich, Y. Shekhtman*, "Tooth fillet profile optimization for gears with symmetric and asymmetric teeth", Gear Technology, **vol. 26**, no. 7, 2009, pp. 73-79.
[14] *X. Tian, M.J. Zuo, K. Fyfe*, Analysis of the vibration response of a gearbox with gear tooth faults, ASME International Mechanical Engineering Congress & Exposition, Anaheim, California, USA, 2004, pp. 785-793.
[15] *D. G. Lewicki*, "Gear crack propagation path studies-guidelines for ultra-safe design", ,Journal of the American Helicopter Society, **vol. 47**, no. 1, 2002, pp. 64-72.
[16] *A. Belsak, J. Flasker*, "Detecting cracks in the tooth root of gears", Engineering Failure Analysis, 14, 2007, pp. 1466-1475.
[17] *J. Kramberger, M. Šraml, S. Glodež, J. Flašker, I. Potrč*, "Computational model for the analysis of bending fatigue in gears", Computers & Structures, 82 (23–26), 2004, pp. 2261-2269.
[18] *E. Ott*, "Chaos in Dynamic Systems", Cambridge University Press, New York, 1993, pp. 277-291.